Multitemporal RADARSAT-2 Polarimetric SAR Data for Urban Land Cover Classification using Object-based Support Vector Machine and Rule-based Approach

Article *in* International Journal of Remote Sensing · September 2012

DOI: 10.1080/01431161.2012.700133

CITATIONS
70

READS
168

2 authors:

Xin Niu
National University of Defense Technology
31 PUBLICATIONS **217** CITATIONS
SEE PROFILE

Yifang Ban
KTH Royal Institute of Technology
143 PUBLICATIONS **1,548** CITATIONS
SEE PROFILE

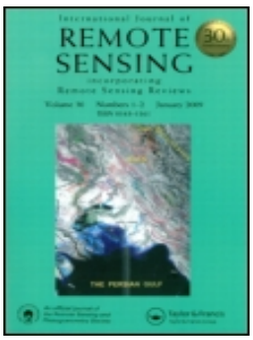

International Journal of Remote Sensing

ISSN: 0143-1161 (Print) 1366-5901 (Online) Journal homepage: http://www.tandfonline.com/loi/tres20

Multi-temporal RADARSAT-2 polarimetric SAR data for urban land-cover classification using an object-based support vector machine and a rule-based approach

Xin Niu & Yifang Ban

To cite this article: Xin Niu & Yifang Ban (2013) Multi-temporal RADARSAT-2 polarimetric SAR data for urban land-cover classification using an object-based support vector machine and a rule-based approach, International Journal of Remote Sensing, 34:1, 1-26, DOI: 10.1080/01431161.2012.700133

To link to this article: http://dx.doi.org/10.1080/01431161.2012.700133

Published online: 10 Sep 2012.

International Journal of Remote Sensing
Vol. 34, No. 1, 10 January 2013, 1–26

Taylor & Francis
Taylor & Francis Group

Multi-temporal RADARSAT-2 polarimetric SAR data for urban land-cover classification using an object-based support vector machine and a rule-based approach

Xin Niu* and Yifang Ban

Division of Geodesy and Geoinformatics, KTH Royal Institute of Technology, Stockholm, Sweden

(*Received 2 March 2011; accepted 13 March 2012*)

We have investigated multi-temporal polarimetric synthetic aperture radar (SAR) data for urban land-cover classification using an object-based support vector machine (SVM) in combinations of rules. Six-date RADARSAT-2 high-resolution polarimetric SAR data in both ascending and descending passes were acquired in the rural–urban fringe of the Greater Toronto Area during the summer of 2008. The major land-use/land-cover classes include high-density residential areas, low-density residential areas, industrial and commercial areas, construction sites, parks, golf courses, forests, pasture, water, and two types of agricultural crops. Various polarimetric SAR parameters were evaluated for urban land-cover mapping and they include the parameters from Pauli, Freeman and Cloude–Pottier decompositions, the coherency matrix, intensities of each polarization, and their logarithm forms. The multi-temporal SAR polarimetric features were classified first using an SVM classifier. Then specific rules were developed to improve the SVM classification results by extracting major roads and streets using shape features and contextual information. For the comparison of the polarimetric SAR parameters, the best classification performance was achieved using the compressed logarithmic filtered Pauli parameters. For the evaluation of the multi-temporal SAR data set, the best classification result was achieved using all six-date data (kappa = 0.91), while very good classification results (kappa = 0.86) were achieved using only three-date polarimetric SAR data. The results indicate that the combination of both the ascending and the descending polarimetric SAR data with an appropriate temporal span is suitable for urban land-cover mapping.

1. Introduction

In the context of global change, urban areas are among the most dynamic due to accelerating urbanization. To make rational policies for sustainable urban development, it is essential to collect up-to-date and reliable information about the current state of urban areas, such as urban land cover/land use through remote sensing. Among many remote-sensing technologies, synthetic aperture radar (SAR) has the capability to acquire data independent of cloud cover or solar illumination conditions. With the launch of advanced spaceborne SAR sensors such as RADARSAT-2 and TerraSAR-X, multi-temporal fully polarimetric SAR data of high resolution have become available. Several recent studies have demonstrated

*Corresponding author. Email: xin.niu@abe.kth.se

ISSN 0143-1161 print/ISSN 1366-5901 online

http://dx.doi.org/10.1080/01431161.2012.700133
http://www.tandfonline.com

the usefulness of polarimetric SAR for urban land-cover mapping (Lombard et al. 2003; Pellizzeri 2003; Pellizzeri et al. 2003; Niu and Ban 2010; Zhang et al. 2010; Zhu et al. 2011). However, urban mapping using such data still remains a challenge due to several factors.

First, the polarimetric properties of urban targets are complex and difficult to interpret. For example, the backscattering from an urban area is a mixture of various scattering mechanisms (Cloude and Pottier 1996; Dong, Forster, and Ticehurst 1997). And the orientation, geometry and material of urban structures can also influence the SAR polarimetric properties (Ainsworth, Schuler, and Lee 2008). To effectively explore SAR polarimetric information, various polarimetric decompositions have been proposed, such as Cloude–Pottier decomposition (Cloude and Pottier 1997), Freeman decomposition (Freeman and Durden 1998), and Pauli decomposition (Cloude and Pottier 1996). Parameters generated by some of those decompositions have been investigated for urban land-cover/land-use mapping (Pellizzeri 2003; Moriyama et al. 2004; Guillaso et al. 2005; Li et al. 2010; Zhang et al. 2010). However, most of these studies focused on the classification of a few urban features using limited polarimetric parameters or extraction of only the urban extent. Very few studies have aimed at detailed urban land-cover mapping using multi-temporal polarimetric SAR data. Furthermore, the efficient combination of high-resolution multi-temporal polarimetric SAR data for such detailed urban mapping has been less investigated due to the lack of multi-temporal high-resolution polarimetric SAR data. In addition, most of the previous studies (Alberga 2007; Alberga, Satalino, and Staykova 2008; McNairn et al. 2009; Li et al. 2010) have compared various polarimetric SAR parameters using a pixel-based classification. However, there are only a few studies on comparisons of these parameters using an object-based approach, especially for urban areas (Niu and Ban 2010).

Second, higher resolution data introduce a higher variance, which is difficult to process using traditional pixel-based methods. Object-based methods (Blaschke 2010), on the other hand, have been increasingly adopted in urban land-cover mapping using SAR data (Hu et al. 2008a; Ban, Hu, and Rangel 2010), since more information such as object features and spatial relationships can be explored in the analysis. Considering the classification performance, several studies have shown that a support vector machine (SVM) can achieve better classification accuracy than other classifiers (Huang, Davis, and Townshend 2002; Pal and Mather 2005; Dixon and Candade 2008). SVM is particularly effective for the classification of multi-temporal or multi-source data, as demonstrated by various studies (Waske and Benediktsson 2007; Lardeux et al. 2009; Niu and Ban 2010; Garcia et al. 2011), since there is no requirement of the statistical model for the data to be classified. The superiority of SVM to other classifiers in the object-based classification of SAR and optical data has also been reported by various studies (Hu et al. 2008a; Tzotsos and Argialas 2008; Waske and van der Linden 2008; Buddhiraju and Rizvi 2010). However, most of those evaluations were conducted on optical data or single-polarization SAR data. Very few studies have investigated object-based SVM for classification of multi-temporal fully polarimetric SAR data. Further, rules on objects' shapes and spatial relationships, etc. could be explored to improve classification when objects from different classes have similar spectral or backscattering properties (Ban, Hu, and Rangel 2010).

Therefore, the overall objective of this research is to investigate multi-temporal RADARSAT-2 polarimetric SAR data for detailed urban land-cover mapping using an object-based SVM in combinations of rules. The specific objectives are:

(1) to evaluate the performances of various polarimetric SAR parameters and the influences of data pre-processing for segmentation and object-based urban land-cover classification;
(2) to investigate object-based SVM and rule-based classification for detailed urban land-cover mapping using polarimetric SAR data; and
(3) to assess the efficient combinations of multi-temporal dual-orbital SAR data for urban land-cover mapping.

2. Study area and data description

The study area is situated in the northern urban–rural fringe of the Greater Toronto Area (GTA), Ontario, Canada. The GTA is the most populous metropolitan area in Canada and is one of the fastest growing urban areas in North America. The urban growth is encroaching on the Oak Ridges Moraine (ORM), an environmentally significant and sensitive area that lies north of Toronto (Furberg and Ban 2008). The main land-use/land-cover types are high-density residential areas (HD), low-density residential areas (LD), industrial and commercial areas (Ind.), construction sites (Cons.), major roads, streets, parks, golf courses, forests, water, pasture and several types of crops.

Six-date RADARSAT-2 fine-beam polarimetric SAR data were acquired in both ascending and descending orbits over the study area during June–September in 2008. These single-look complex products include observations from HH, HV, VH, and VV polarizations with a nominal pixel spacing of 4.7 and 5.1 m in the range and azimuth directions, respectively. The centre frequency of this beam mode is 5.4 GHz, i.e. C-band. The areas covered by the ascending and descending observations are marked in red in Figure 1.

The six-date data could be divided into two groups according to ascending or descending orbits. All data were collected under similar incident angles; thus, the difference between the images from the two orbits is mainly introduced by the radar look directions. The data from ascending and descending orbits are expected to complement each other by observing urban areas from two different look directions. The SAR data were acquired during the vegetation season to improve the differentiation between built-up classes and vegetation classes. The characteristics of these SAR images are summarized in Table 1.

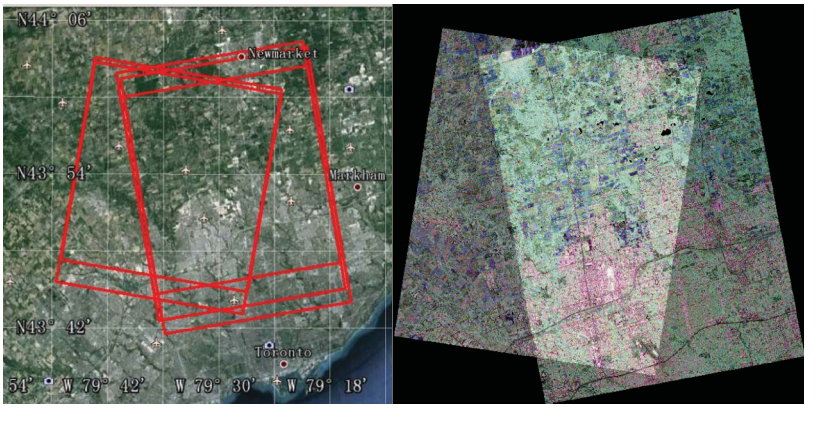

Figure 1. The study area: rural–urban fringe of GTA, Ontario, Canada.

Table 1. RADARSAT-2 Fine Quad-Pol SAR Imagery.

Date	Orbit mode	Incident angle (°)	Code number
11 June 2008	Ascending	40.18–41.59	A1
19 June 2008	Descending	40.22–41.62	D1
5 July 2008	Ascending	40.18–41.60	A2
6 August 2008	Descending	40.20–41.61	D2
22 August 2008	Ascending	40.17–41.59	A3
15 September 2008	Ascending	40.17–41.59	A4

3. Methodology

The proposed multi-temporal classification scheme is illustrated in Figure 2. First, the multi-date raw SAR data were geometrically corrected and registered to the same database. Next, various polarimetric parameters were generated for each date. After that, the geo-referenced multi-temporal image stacks were segmented into objects. Then, these objects were classified into 11 land-use/land-cover categories using SVM based on their multi-temporal polarimetric features. Afterwards, a set of rules were applied to further refine the SVM results and to extract major roads and streets. Detailed descriptions of each step in the experiment are given in the following sections.

In the experiments, the popular open source SVM software, LIBSVM (Chang and Lin 2010), was used as the SVM classifier, while segmentation and the object-based rules were implemented in Definiens eCognition/Developer.

For the comparison of various polarimetric parameters, the object-based SVM classifications were performed on every polarimetric SAR parameter set from the ascending data stack (four-date) or descending data stack (two-date). These results were compared to identify the best parameter set. For the comparison of multi-temporal dual-orbit combinations, the best polarimetric parameter set selected from the above comparison was used to evaluate the classification results of different date and orbit combinations. This comparison was conducted on the overlapping area of all ascending and descending images.

3.1. Geometric correction of SAR images

To remove the relief displacements introduced by the terrain and the opposite look directions, each of the raw SAR data was ortho-rectified using RADARSAT-2 orbital parameters

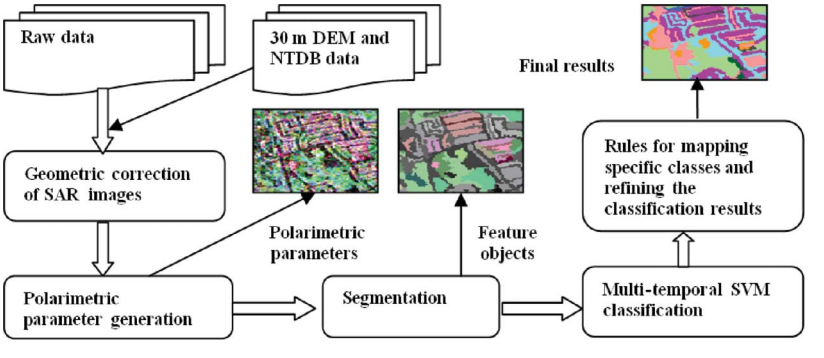

Figure 2. Multi-temporal object-based classification scheme.

and a digital elevation model (DEM) with a resolution of 30 m by DMTI Spatial Inc. Then the multi-temporal data were registered to the vectors in the National Topographic Database (NTDB).

3.2. Polarimetric SAR parameter sets

To evaluate the performances of various polarimetric SAR parameters for object-based urban land-cover classification, several typical polarimetric parameter sets from both coherent and incoherent decomposition methods were selected for comparison, as presented in Table 2. Brief introductions to some of the polarimetric parameters are provided in the following.

As the base of many other decomposition parameters, the Hermitian coherency matrix **T** was first extracted. Under the reciprocal assumption of the scattering matrix (HV = VH), the 3 × 3 coherency matrix **T** is constructed by the Pauli target vector (Cloude and Pottier 1996):

$$p = \frac{1}{\sqrt{2}}[\mathrm{HH} + \mathrm{VV}\ \mathrm{HH} - \mathrm{VV}\ 2\mathrm{HV}]^{\mathrm{T}}, \tag{1}$$

$$\mathbf{T} = \boldsymbol{p}\boldsymbol{p}^{*\mathrm{T}}. \tag{2}$$

The raw Pauli parameters are the three diagonal elements of the coherency matrix **T**. They are calculated by $0.5|\mathrm{HH} + \mathrm{VV}|^2$, $0.5|\mathrm{HH} - \mathrm{VV}|^2$ and $2|\mathrm{HV}|^2$. Freeman decomposition (Freeman and Durden 1998) models the polarimetric characters of the backscattering by three scattering mechanisms such as double bounce (D), odd bounce (O) and volume (V). Cloude–Pottier decomposition (Cloude and Pottier 1997) interprets the polarimetric properties through three parameters, entropy (H), anisotropy (A) and alpha (a), generated from the eigenvalues and eigenvectors of the coherency matrix. Entropy measures the purity of the scattering types. Alpha is an indicator of the averaged scattering mechanism. Under the reciprocal assumption, there are three scattering mechanisms represented by the three eigenvectors. Besides the major scattering mechanism, the anisotropy indicates the relationship between the other two minor scattering mechanisms. For incoherent decomposition methods such as Freeman and Cloude–Pottier decomposition, a sample average operation, known as a multi-look process, is required for obtaining unbiased estimation. For Cloude–Pottier decomposition, a 7 × 7 multi-look size was employed as recommended by Lee et al. (2008), while for Freeman decomposition, a 3 × 3 multi-look size was used for generating sharp and unflattering images. These above-described parameters were also compared with the traditional polarimetric SAR intensities.

Table 2. Selected polarimetric parameter sets for comparisons.

Parameter set (code)	Elements	Parameter set (code)	Elements
Intensity (I)	$\|\mathrm{HH}\|^2$, $\|\mathrm{HV}\|^2$, $\|\mathrm{VV}\|^2$	Compressed logarithmic Pauli (CLP)	$(\log(\text{raw Pauli}))_{\text{8-bit}}$
Logarithmic intensity (LI)	log(intensity)	Compressed logarithmic filtered Pauli (CLFP)	$(\log(\text{filtered Pauli}))_{\text{8-bit}}$
Coherency matrix (**T**)	**T**	Freeman (Freeman)	D, O, V
Raw Pauli (RP)	**T**11, **T**22, **T**33	Cloude–Pottier (Pottier)	H, A, a
Logarithmic Pauli (LP)	$\log(\text{raw Pauli})_{\text{16-bit}}$		

3.3. SAR data processing

Regarding the data processing approach to improve the classification result, Rignot, Chellappa, and Dubois (1992) reported two advantages of using the logarithmic data: (1) depression of the noise and (2) balancing the driven force from different polarizations in the clustering process. Thus, the comparisons of the data with their logarithmic form were carried out. Previous research also reported the efficiency of using the compressed remote-sensing data for classification (Lukin et al. 2006) and for segmentation (Hu et al. 2008a, 2008b). Hence, we also conducted comparisons involving compressed and filtered data. We proposed a data set called the compressed logarithmic filtered Pauli parameter set for segmentation and classification. This data set includes Pauli parameters first filtered by the refined Lee filter (Lee 1981) with a window size of 7×7, and then have their logarithm form truncated from 16-bit to 8-bit through linear scaling. To remove the outlier pixels and get the main part of the data distribution stretched in the whole data value range, 1–2% of the pixels in the lower and upper limit of the data range were trimmed in the scaling. One example of the data distributions before and after scaling is given in Figure 3.

Therefore, for urban land-cover classification, we focus on the comparisons of the SAR polarimetric parameters and effects of data processing in the following perspectives.

(1) Efficiency of various polarimetric SAR parameters from different polarimetric decompositions: in this case, the efficiencies of the Freeman, Cloude–Pottier, Pauli, intensity, and coherency matrix parameters were compared.
(2) Efficiency of using incomplete information: the coherence matrix represents the whole information of the recorded backscattering, while the raw Pauli data are just the diagonal elements of the coherence matrix. To see the effects of using partial information, the mapping results using the raw Pauli data were compared with the results using all the elements from the coherence matrix.
(3) Efficiency of using a logarithm in the data processing: for this purpose, the mapping results of using log intensity were compared with the results using raw intensity. The results of using log Pauli were compared with those using raw Pauli.
(4) Efficiency of data compression: mapping results of using the compressed (scaled and truncated to 8-bit) logarithmic Pauli were compared with the results using logarithmic Pauli.
(5) Efficiency of filtering: mapping results of using the compressed logarithmic filtered Pauli were compared with the results using compressed logarithmic Pauli.

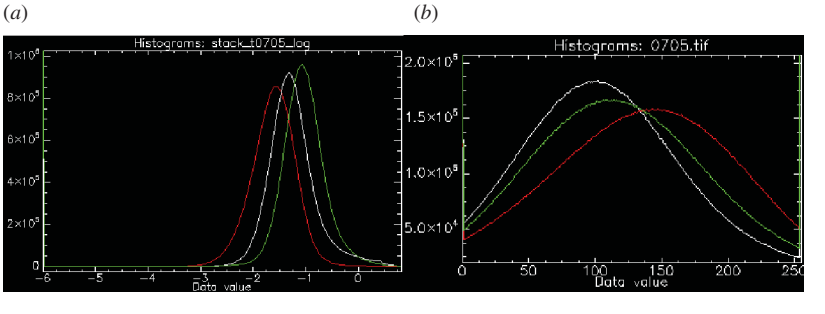

Figure 3. Data distributions of the logarithmic Pauli parameters (*a*) and the compressed logarithmic Pauli parameters (*b*) (white: $0.5|HH - VV|^2$; red: $2|HV|^2$; green: $0.5|HH + VV|^2$).

3.4. Segmentation of polarimetric SAR images

In an object-based classification, successful segmentation of meaningful objects is essential to the final mapping results. A perfect meaningful object should represent just one defined class, with no other class mixed inside. Furthermore, it should be as big as possible and have the typical shape of the feature it represents. For example, in this study, we were interested in the urban land cover. Thus, the low-density and high-density residential areas were the interested classes, not individual houses or trees. Hence, a compact block of buildings should be segmented as one high-density residential object. The area which consists of sparse small houses, lawns and trees should be segmented as one low-density residential object. And wide roads and streets should be cut as linear segments with proper width, but not into fragmented small pieces. In this study, the multi-resolution segmentation algorithm introduced by Baatz and Schäpe (2000) was employed, and the segmentation processes were implemented in Definiens eCognition/Developer.

For SAR image segmentation, the previous study by Hu and Ban (2008a, 2008b) demonstrated the superiority of using the compressed 8-bit data rather than the raw 16-bit data. Therefore, the 8-bit compressed data were selected for segmentation in this study. Performances of the segmentations by various polarimetric parameters with different pre-processing steps were visually compared. Figure 4 presents some selected segmentation results, and shows that the multi-temporal compressed logarithmic filtered Pauli parameters could generate better segmentation results than the others. By the same pre-processing, the compressed logarithmic filtered intensity image could generate segmentation results very similar to those generated by the compressed logarithmic filtered Pauli. Without filtering or scaling, however, segmentation results from Pauli or intensity images are unacceptable (Figure 4(*b*)). Even after filtering, logarithm and scaling, the Freeman and Cloude–Pottier parameters could not generate satisfactory segments (Figures 4(*c*) and (*d*)). The results are much poorer for Freeman and Pottier parameters without pre-processing.

Since most of the polarimetric parameters and their pre-processed forms could not generate meaningful segments, segmentation results from the compressed logarithmic filtered Pauli parameters were selected based on visual comparison as discussed earlier. These segmentation results were used to segment each polarimetric parameter set in order to compare their capacities for urban land-cover classifications. Actually, the parameter comparisons were performed using the ascending and descending data stacks.

For the comparison of the multi-temporal combination efficiencies, each combination has its own segmentation generated using the compressed logarithmic filtered Pauli parameters from its date members.

3.5. Selection of training and validation samples

For the object-based classification, training objects and validation pixels were randomly selected based on the QuickBird images of 2008 and field data. As the focus of this research is urban land cover, agricultural crops were grouped into crop 1 and crop 2 based on their multi-temporal backscattering properties.

For comparisons of the polarimetric parameters, we prepared two training and validation sets using the ascending and descending data stack. For comparisons of the multi-temporal combination efficiencies, every date combination has its own training set. This is due to the fact that every combination has its unique segmentation based on the data of its member dates; thus, it is impossible to set the same object samples for different date combinations. However, these training objects were selected from the same locations and

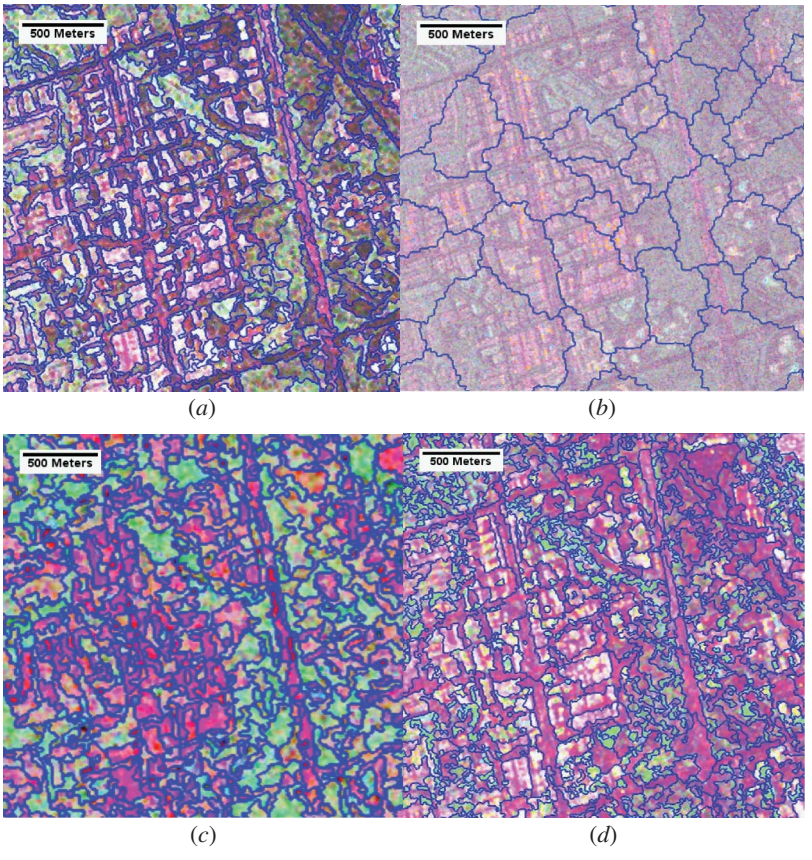

Figure 4. Segmentation results of (*a*) compressed logarithmic filtered Pauli image, (*b*) logarithmic filtered Pauli image without scaling, (*c*) compressed logarithmic filtered Pottier image and (*d*) compressed logarithmic filtered Freeman image.

from the same observed targets as much as possible. Also, the numbers of training objects for every combination were kept the same.

One validation sample set was used for evaluation of the classifications from these multi-temporal combinations. The validation samples were randomly selected pixels evenly distributed over the study area. The number of validation pixels for each class was determined according to the proportion of the class and the balance between the other classes. In the evaluation, we used both the overall accuracy and kappa coefficient to assess the classification results.

The number and distributions of training and validation samples are given in Tables 3 and 4. The number of training objects for each class is about 10–20. Some classes such as water, golf courses or construction sites had less training objects, as there were not so many objects for these classes. Unlike the pixels, features of the objects belonging to the same class do not vary too much. In addition, SVM presents a strong ability in dealing with such small-sized training sets (Foody and Mathur 2004).

3.6. Object-based SVM classification

The principle of SVM classification can be briefly described as follows. Through mapping the input vectors into the high-dimension space, SVM searches for the optimal hyper-plane

Table 3. Training object number of each class.

	LD	HD			Ind.				F	Cons.	Pk.	Pt.	G	W	C1	C2	
	LD	HD1	HD2	HD3	I1	I2	I3	I4	F	Cons.	Pk.	Pt.	G	W	C1	C2	Total
A	11	20	12	8	12	9	16	15	22	8	16	10	15	8	12	14	208 (0.6%)
D	10	15	15	7	9	6	9	12	18	11	15	7	18	8	14	17	191 (0.5%)
O	11	17	13	5	8	9	13	13	16	6	12	9	11	7	10	10	170 (0.8%)

Notes: 'A' and 'D' indicate the parameter comparisons on the ascending and descending data stack. 'O' indicates the multi-date efficiency comparisons on the overlapping area of all the images. 'LD' indicates low-density area, 'HD' indicates high-density area, 'Ind.' indicates industry and commercial area, 'F' indicates forest, 'Cons.' indicates construction site, 'Pk.' indicates park, 'Pt.' indicates pasture, 'G' indicates golf, 'W' indicates water and 'C1' and 'C2' indicate crop 1 and crop 2. Percentages indicate the number of sample objects to the number of total classified objects.

Table 4. Validation pixel number of each class.

	Parameter comparisons on ascending data	Parameter comparisons on descending data	Multi-date efficiencies on overlapping area
LD	27 192 (0.08%)	23 109 (0.07%)	22 977 (0.11%)
HD	58 008 (0.19%)	49 934 (0.16%)	46 105 (0.23%)
Park	63 256 (0.2%)	38 735 (0.12%)	36 017 (0.18%)
Ind.	49 602 (0.16%)	38 478 (0.12%)	38 163 (0.19%)
Cons.	15 278 (0.05%)	13 478 (0.04%)	13 289 (0.06%)
Street	45 930 (0.15%)	32 815 (0.10%)	30 815 (0.15%)
Road	44 036 (0.14%)	27 242 (0.09%)	26 151 (0.13%)
Golf	26 230 (0.08%)	14 587 (0.05%)	14 283 (0.07%)
Water	9 141 (0.03%)	8 941 (0.03%)	8 820 (0.04%)
Pasture	41 538 (0.13%)	71 518 (0.23%)	40 342 (0.20%)
Forest	57 723 (0.19%)	57 011 (0.18%)	56 573 (0.28%)
Crop 1	36 748 (0.12%)	59 036 (0.19%)	35 433 (0.18%)
Crop 2	82 435 (0.27%)	98 995 (0.31%)	66 288 (0.33%)
Total	557 117 (1.8%)	533 879 (1.7%)	435 256 (2.2%)

Note: Percentages indicate the number of validation pixels to the number of total pixels on the classified map.

to separate the training vectors of two classes into two sub-spaces. Therefore, the class of the test vector will be decided according to which sub-space it will be mapped in. Therefore, SVM is originally a binary classifier. In this research, we employed the SVM tool LIBSVM using the one-against-one approach (Hsu and Lin 2002). There are many kernel functions used to map the input vectors into the high-dimension space. In our study, the radial basis function (RBF) has been selected as the mapping kernel function:

$$k(x, x_i) = \exp\left(-\gamma \left\|x - x_i\right\|^2\right), \ \gamma > 0, \tag{3}$$

where x is the input data vector, x_i is the training data vector of sample i. When using SVM for classification with the RBF kernel, optimization of two parameters is necessary to improve the predictive accuracy: the penalty value C and kernel parameter γ. In SVM, the penalty C controls the trade-off between the training error and model complexity. In our study, the best parameters were selected from a limited searching grid through a cross-validation process. More information about SVM techniques is given in Muller et al. (2001).

In this study, high-density residential areas, low-density residential areas, industrial and commercial areas, construction areas, forests, golf courses, parks, water, pasture and two types of crops were classified using the multi-temporal polarimetric features with SVM. In practice, in the SVM classification, many sub-types were defined for specific classes. For example, diverse polarimetric behaviours of the industrial and commercial areas could be observed due to buildings' orientation, alignment and external materials. Thus, the industrial and commercial areas could be divided into several sub-classes. To achieve better classification results, those sub-classes were separately classified. After the SVM classification, these sub-classes were merged into the super-class they belong to.

To classify the objects using a specific polarimetric parameter set, the mean and the standard deviation of each parameter of that set for each object were calculated as the object's feature input into the SVM. For the multi-date data stack, a multi-date string of such means and standard deviations was obtained for each object. Therefore, the elements of the object's feature vector input into the SVM consisted of that multi-date mean and standard deviation string and the brightness and maximum difference (Max.Diff) indicators. Brightness $\overline{C}(v)$ is defined as

$$\overline{C}(v) = \frac{1}{w^B} \sum_{k=1}^{K} w_k^B \overline{C}_k(v), \tag{4}$$

where w_k^B is the brightness weight of the kth parameter layer in the multi-temporal stack; in this study, brightness weight values were all set as 1. $\overline{C}_k(v)$ is the mean of the kth parameter in object v. K is the number of the total parameter layers in the multi-date stack. And

$$w^B = \sum_{k=1}^{K} w_k^B. \tag{5}$$

Max.Diff is given as

$$\frac{\max\limits_{i,j \in K_B} \left| \overline{C}_i(v) - \overline{C}_j(v) \right|}{\overline{C}(v)}, \tag{6}$$

where $K_B = \left\{ k \in K | w_k^B = 1 \right\}$; in this study, it is equal to K.

For example, to classify the objects by Freeman parameters in the descending data stack, the elements of the input vector are the 'odd bounce' mean, 'double bounce' mean and 'volume' mean of 19th June and 6th August, the corresponding standard deviations of these parameters and the brightness and Max.Diff of these means.

3.7. Rule-based classification

To improve the SVM classification results and to extract major roads and streets, a set of rules were applied. The relationship of the SVM classification and the rule-based approach is illustrated in Figure 5. The rule-based classification was implemented in Definiens eCognition.

Since the SAR backscattering properties of major roads and streets are influenced by their neighbouring targets, they were extracted mainly by their particular shape features and typical spatial relationships with other classes. While the object-based SVM performed on

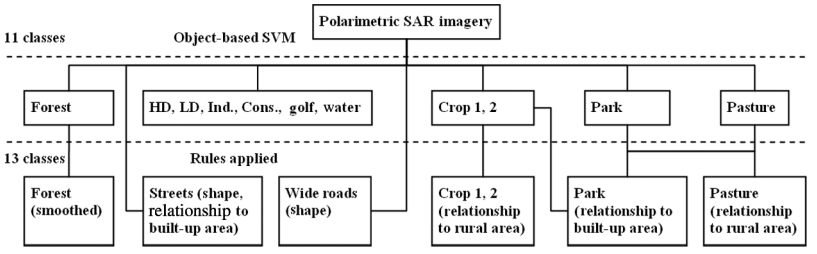

Figure 5. SVM and rule-based classification scheme.

the segmentation layer of scale 50, the major roads were extracted on the segmentation layer of scale 100. Long and moderately wide segments with fewer curves were the candidates for major roads. Roads generally have low backscatter compared to other classes in the cross-polarization channel HV. Streets were defined as narrow curving segments within the built-up areas, since the street object is usually formed by the connected line type segments in different directions. These shape properties of the streets were expressed using two shape parameters used in eCognition, namely roundness and rectangular fit (Definiens 2011). The roundness feature describes how similar an image object is to an ellipse. It is calculated by the difference of the enclosing ellipse and the enclosed ellipse. The rectangular fit feature describes how well an image object fits into a rectangle of similar size and proportions. Streets usually have high roundness but low rectangular fit with proper width. In addition, parks and pastures are confused with each other due to their similar low backscatter in SAR images. The mapping of parks and pastures was refined by the relationship between these classified objects and the built-up areas. Thus, SVM-classified parks in rural areas were converted to pastures. Similarly, pastures and crops in urban areas were corrected into parks. Then the final mapping result is further improved by removing the isolated small objects within the forest class. Formal definitions of those rules are given as follows:

Extraction of Major Roads and Streets
Major Roads:
(a) Ratio of length to width > threshold_L/W, and
Lowest_value < Width < Highest_value, and
backscattering in HV < threshold_HV, or
(b) Ratio of length to width is extremely high, or
(c) Length is extremely long, and
Lowest_value < Width < Highest_value

Streets:
(a) Roundness*(1-Rectangular Fit) > threshold value, and
Lowest_value < Width < Highest_value, or
(b) Ratio of length to width > threshold_L/W, and
Lowest_value < Width < Highest_value,

Refinement of Park and Forest
Park:
Pasture, crops with small distance to the built-up area.
Pasture:
(a) Park with long distance to the built-up area.

Forest:
(a) Objects with small area enclosed in the Forest.

3.8. *Significance test*

To evaluate the significance of the differences in classification accuracy, McNemar's test (Bradley 1968; Agresti 1996) has been employed in many previous studies on remote sensing (Debeir et al. 2002; Gao et al. 2006). In this study, McNemar's test was used to evaluate the significance of the differences between similar classification results in the polarimetric parameter comparisons and multi-temporal combination comparisons.

4. Results and discussion

In this research, various polarimetric SAR parameters were evaluated and the best parameter set was then selected to evaluate the efficiency of multi-temporal SAR data for urban land-cover classification. Results from multi-temporal SAR combinations are presented and discussed.

In the following comparisons, both the results using object-based SVM only and results using the SVM and rule-based approach are given. Note that the SVM results are assessed by the 11 classes that were directly classified by the object-based SVM according to their multi-temporal polarimetric properties while the SVM and rule-based results have 13 classes by adding two classes: major roads and streets.

4.1. *Comparison of different polarimetric SAR parameter sets*

The classification results of various polarimetric SAR parameters and the processing steps are illustrated in Figures 6 and 7. The comparisons were conducted on the ascending and descending data stacks, since each data stack covers much more area than the overlapped part of the whole data set for study. Further, a single looking direction data stack could also avoid the influences introduced by the dual orbits when comparing the results of the polarimetric parameters.

From both the ascending and the descending data, the following facts could be observed.

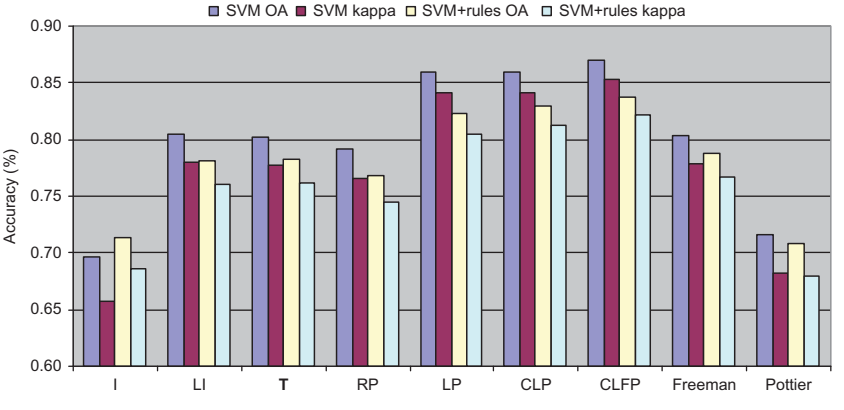

Figure 6. Comparison of various polarimetric SAR parameters on the ascending data stack.

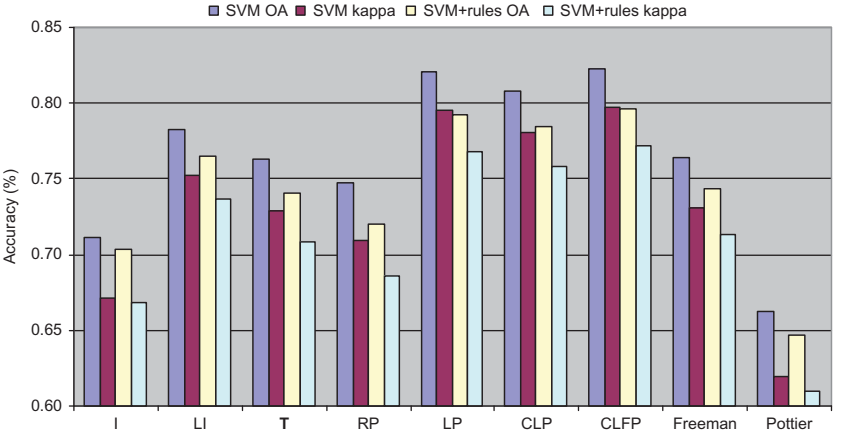

Figure 7. Comparison of various polarimetric SAR parameters on the descending data stack.

(1) In terms of the SAR polarimetric parameters.
For different polarimetric decompositions, Freeman parameters could generate results similar to those of the coherency matrix. They could even compete with the logarithmic intensity parameters. Both are better than the other polarimetric parameters without processing. However, the potential of further processing on the Freeman parameters was not as high as that on the Pauli parameters, which could also be observed by the segmentation results of their processing form (Figures 4(*a*) and (*d*)).

The higher performance of the coherency matrix was expected, since it contains whole polarimetric information. Considering the effects of using partial polarimetric information, the raw Pauli parameters as the diagonal elements of the coherency matrix (**T**) could generate results very similar to the use of all matrix elements, although the coherency matrix is slightly better than the raw Pauli. The raw Pauli is better than the intensity. The superiority of the Pauli parameters is probably due to the introduced phase information which is not contained in intensity.

The Cloude–Pottier parameters yielded lower accuracy than the other parameters. Only in the ascending stack, a slight improvement is observed compared with the intensity parameters. The inefficiency of using Cloude–Pottier parameters directly for classification has also been reported in several previous studies (Alberga 2007; Alberga, Satalino, and Staykova 2008; Trisasongko 2010). Possible explanations are the following: first, the Cloude–Pottier parameters were derived from the eigenvalues and part of the eigenvectors of the coherency matrix, and thus part of the polarimetric information was not used in classification. Second, the parameter anisotropy is noisy when the entropy parameter is low; from the practical point of view, anisotropy is meaningful when entropy is high. Thus, for those low-entropy classes, the anisotropy parameter is not efficient.

(2) In terms of data pre-processing.
Based on the previous parameter comparisons, Pauli parameters were selected for further processing. Generally, the processed parameters were better than the unprocessed ones. The compressed logarithmic filtered Pauli (CLFP) produced the best results. All of the Pauli logarithmic forms (i.e. LP, CLP, CLFP) are obviously better than the other raw polarimetric parameters. Although the results between these logarithmic forms are similar, significant differences between them were found by

the McNemar tests. The only exceptions are the results of LP and CLP in ascending comparison.

Specifically, the logarithmic data are obviously better than the raw data, which is demonstrated by the comparison between LP and raw Pauli (RP), and comparison between logarithmic intensity (LI) and intensity (I). The LI could compete with the coherency matrix (**T**), while the LP is even better than the coherency matrix (**T**).

In terms of data compression, the results of the compressed one, CLP, are similar to those of LP. The McNemar's test between LP and CLP in ascending comparison is not significant. Although the compression suppresses part of the information, it may also suppress the speckles. Further, the compression could balance the classification-driven force between channels. Thus, compressed data with a proper compression rate could generate similar or even better results than the uncompressed data, while the storage size was simultaneously reduced.

In terms of filtering, although CLFP are very similar to CLP, i.e. the unfiltered one, significant difference is demonstrated by the McNemar test. The similarity is due to the approximation of the mean values within the object before and after filtering. However, in most of the situations, the filtered data are slightly better than the unfiltered ones.

To further understand the performances of various parameters for urban land-cover classification, producer and user accuracies using only SVM in ascending data comparison are given in Figures 8 and 9. For example, an obvious improvement by logarithm processing is observed not only on many high-scattering built-up classes but also some low-scattering classes such as pastures and construction sites. For the majority of classes, a similarity between the coherency matrix (**T**) and the raw Pauli (RP) was maintained, and the best performances were frequently found from the processed Pauli set (LP, CLP, CLFP). The Cloude–Pottier parameters produced relatively lower classification accuracies for most classes, especially for those low-scattering categories such as golf course, pasture, park and water. However, construction sites and crops could be well identified by Cloude–Pottier. Freeman parameters have shown good ability in identifying high-density residential areas from industry as well as mapping forest. Similar trends are observed using the descending data set as well.

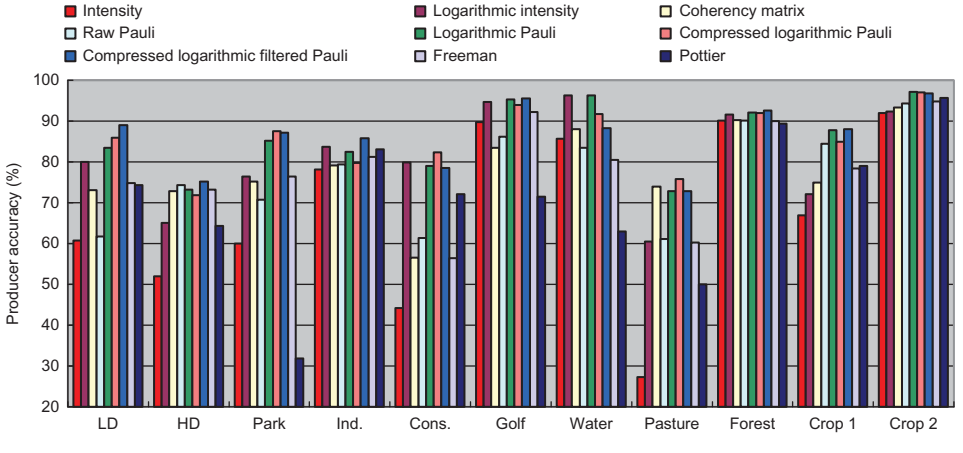

Figure 8. Producer accuracy comparison of polarimetric parameters for land covers on the ascending data stack.

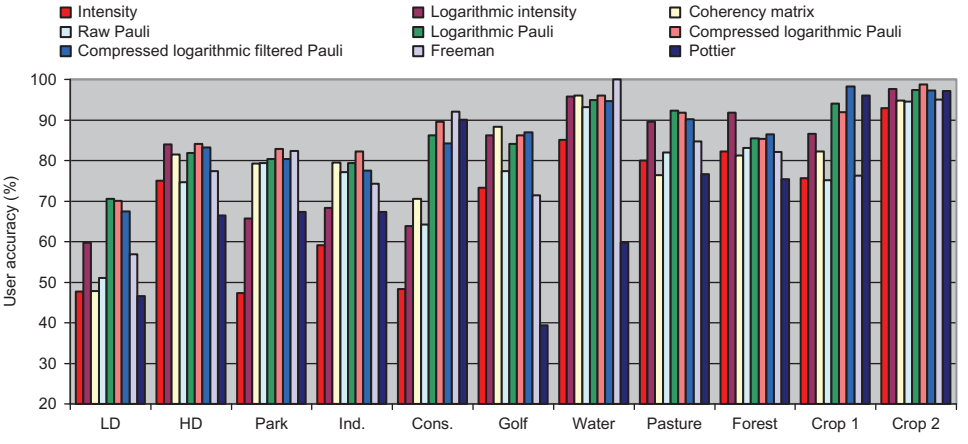

Figure 9. User accuracy comparison of polarimetric parameters for land covers on the ascending data stack.

4.2. Comparison of the multi-temporal SAR data efficiency

The efficiency of the selected SAR data for multi-temporal classification depends not only on the quality of each selected single date but also on the efficiency of the combinations. To fairly compare the multi-temporal efficiencies, each combination had its own segmentation using the compressed logarithmic filtered Pauli parameters from its member dates. Since the best classification was observed using the compressed logarithmic filtered Pauli parameters, it is selected as the input feature of the classifications and subsequent multi-temporal comparisons. For convenient description, each date is simply indicated by its code from Table 1.

Similar to previous studies (Ban 2003; Ban and Wu 2005), we found that all the single dates have very poor results, with kappa ranging from 0.51 to 0.67. The ascending data had slightly better performance than the descending ones. The major deficiency of the descending data originates in the confusion between the low-density areas and the forest. However, the descending data had better performance for mapping high-density areas. Therefore, complement information could be explored by combining the ascending and the descending data. Since the incident angles were almost the same, while the urban area was relatively stable in the observation time span, the difference of the multi-date data in the same orbital mode was mainly caused by the temporal characters of the vegetation.

The classification accuracies of the multi-temporal combinations are presented in Table 5. All the results of the combination examples discussed below have significant differences, which are demonstrated by the McNemar test. Based on Table 5, the following phenomena could be observed.

(1) Accuracy could be improved by adding more data to the multi-temporal combination data set. Generally, three-date data is better than two-date data, and four-date is better than three-date. Multi-date data not only provide more information on the classification, but also bring better segmentations, which would further influence the performance of the object-based classification. Although the best result (kappa = 0.91) was achieved using all of the six-date data, very good results (kappa = 0.86) could be achieved using only three-date data.

Table 5. Comparison of selected multi-temporal combinations (%).

		A1 + D1	A2 + D1	A3 + D1	A4 + D1	A1 + D2	A2 + D2	A3 + D2
SVM	OA	0.80	0.80	0.83	0.84	0.85	0.84	0.78
	kappa	0.77	0.77	0.80	0.81	0.83	0.82	0.75
SVM + rules	OA	0.76	0.76	0.80	0.80	0.81	0.80	0.75
	kappa	0.74	0.74	0.78	0.78	0.79	0.78	0.73
		A4 + D2	D12	A12	A23	A123	A124	A234
SVM	OA	0.78	0.80	0.78	0.81	0.82	0.84	0.81
	kappa	0.75	0.77	0.75	0.78	0.79	0.82	0.78
SVM + rules	OA	0.75	0.76	0.75	0.78	0.79	0.81	0.78
	kappa	0.72	0.73	0.73	0.75	0.77	0.78	0.76
		A1 + D12	*A2 + D12*	*A3 + D12*	*A4 + D12*	A12 + D1	A12 + D2	A12 + D12
SVM	OA	0.85	***0.88***	***0.88***	*0.88*	0.83	0.86	0.86
	kappa	0.83	***0.86***	***0.86***	*0.86*	0.81	0.85	0.84
SVM + rules	OA	0.81	***0.83***	***0.85***	*0.83*	0.80	0.83	0.83
	kappa	0.79	***0.82***	***0.83***	*0.82*	0.78	0.81	0.81
		A123 + D1	A123 + D2	A123 + D12	A124 + D12	A134 + D12	A1234	*A1234 + D2*
SVM	OA	0.87	0.89	0.89	0.90	0.91	0.85	***0.92***
	kappa	0.85	0.88	0.88	0.89	0.89	0.84	***0.91***
SVM + rules	OA	0.83	0.85	0.86	0.86	0.86	0.82	***0.90***
	kappa	0.81	0.83	0.84	0.85	0.85	0.80	***0.89***

Notes: OA, overall accuracy. The bold and italic font highlights the efficient 3 date data combination examples of A1 + D12 and A3 + D12 with comparison to the best result of A1234 + D12 which used six-date data.

(2) Complementary information from the ascending and descending data is important in the multi-temporal classifications. For example, it is observed that all the ascending data stack of four dates A1234 is not as good as some three-date combination of data from both orbits, such as A2 + D12, A3 + D12 and A4 + D12. The descending data stack D12 is not as good as some two-date combinations from both orbits such as A3 + D1 and A2 + D2.
(3) The temporal relationship between the selected data is significant in the multi-temporal classifications, since more difference was observed from a wider time span. For example, A4 + D1 is better than A1 + D1. This is due to the fact that the time span between A4 and D1 is wider than the other.

To further understand the efficiencies of the multi-temporal classification, confusion matrices of the best three-date combination A3 + D12 and all dates A1234 + D12 using object-based SVM are presented in Tables 6 and 7. By providing more multi-temporal information, classification of all six-date SAR data obviously improved the classification accuracies for most of the classes. Similar good results could also be found for some classes on the best three-date results in terms of both the user's and producer's accuracy. Generally, the natural classes benefited more from the additional data than the urban classes. For the urban classes, the low-density class was significantly improved by reducing the commission to industry and omission by high-density areas. This could be due to the improvement of the segmentation results by more data on such heterogeneous areas. However, confusion between the high density and industry still remained. Improvement of the construction site was not evident. For vegetation classes, classifications of crops were definitely improved. Confusion between the low-backscattering classes was reduced, resulting in the improvement of the pasture, golf, park and water.

When applying the rules, two additional classes, major roads and streets, could be extracted with a reasonable accuracy. The accuracies of some specific classes were improved, although the overall accuracy was lower than that of only object-based SVM. This is mainly due to the addition of two extra classes, which also introduces confusion with other urban classes. For the majority of classes, the confusion situations among oneanother are similar to that which occurred before applying the rules. However, improvement of the forest is observed. The park class has increased user accuracy and decreased producer accuracy, while the pasture class has increased producer accuracy and decreased user accuracy. Nevertheless, in most of the situations, this refinement for park and pasture has increased the overall accuracy. Street has most omissions in the urban categories, the missed detection being mostly due to difficulty in segmentation of the streets from the urban area. Since the street and road classes were extracted by their shape features, the segmentation result is essential for identifying those classes by rules. Therefore, combinations of SAR data from more dates produced better mapping of road and street since better segmentation could be achieved by adding more data. Figure 10 shows several classification examples of the comparison between the SVM-only results and results by SVM and rules.

4.3. Major contribution of this research

To put our research in context, a comparison is made between our findings and the findings of previous studies on urban land-cover mapping using polarimetric SAR data (Table 8).

Table 6. Confusion matrix of the multi-date combination A3 + D12 classification result by using compressed logarithmic filtered Pauli parameters by only object-based SVM (%).

	LD	HD	Park	Ind.	Cons.	Golf	Water	Pasture	Forest	Crop 1	Crop 2
LD	87.86	7.51	2.11	3.39	1.17	0.03	0	0.07	3.15	0	0
HD	9.63	83.33	0.09	12.65	0	0	0.01	0	0.89	0.06	0
Park	1.36	1.63	89.42	1.23	3.17	8.84	0.03	20.18	1.11	0.07	0.81
Ind.	0	6.95	0.01	82.31	0.02	0	0	0	0.13	0	0
Cons.	0	0.24	0.48	0	91.83	0.92	0.03	0.03	0	0.12	0.79
Golf	0	0	2.41	0	1	85.07	6.29	0.97	0	0	0
Water	0	0	0.35	0.32	0	3.92	93.63	0	0.07	0	0
Pasture	0.1	0	0.34	0	0.13	1.06	0	76.22	0.39	1.65	0.48
Forest	1.05	0.34	3.26	0.06	0.02	0.17	0	0.42	94.17	3.97	6.93
Crop 1	0	0	1.54	0	0.64	0	0	1.91	0.09	93.19	0.23
Crop 2	0	0	0	0.04	2.02	0	0	0.2	0	0.94	90.75
Producer	87.86	83.33	89.42	82.31	91.83	85.07	93.63	76.22	94.17	93.19	90.75
User	72.95	83.49	71.95	90.53	92.5	86.18	90.72	95.55	87.23	95.35	98.85

Table 7. Confusion matrix of the multi-date combination A1234 + D12 classification result by using compressed logarithmic filtered Pauli parameters by only object-based SVM (%).

	LD	HD	Park	Ind.	Cons.	Golf	Water	Pasture	Forest	Crop 1	Crop 2
LD	94.06	8.14	2.52	0.57	2.58	0.15	0	0.29	2.41	0	0.08
HD	4.46	78.46	0.1	5.83	0	0.22	0	0	2.29	0	0
Park	0.77	0.01	90.38	0.43	3.48	1.65	1.49	5.31	0.33	0.05	0
Ind.	0.1	13.4	0.7	92.92	0.07	0	0	0	0.1	0	0
Cons.	0	0	0.33	0	88.14	0	0	0.35	0	0	0.75
Golf	0	0	3.75	0	4.45	96.63	7.68	1.14	0	0	0
Water	0	0	0	0	0	0.76	90.84	0	0	0	0
Pasture	0.03	0	0.01	0	0	0.54	0	91.99	0.16	0.39	0
Forest	0.58	0	1.32	0.25	0	0.06	0	0.34	94.49	1.99	0.1
Crop 1	0	0	0.79	0	0	0	0	0.28	0.22	97.55	0.71
Crop 2	0	0	0.09	0	1.29	0	0	0.3	0	0.02	98.36
Producer	94.06	78.46	90.38	92.92	88.14	96.63	90.84	91.99	94.49	97.55	98.36
User	76.13	88.69	90.24	84.47	93.91	81.76	98.67	99.16	97.05	97.2	99.5

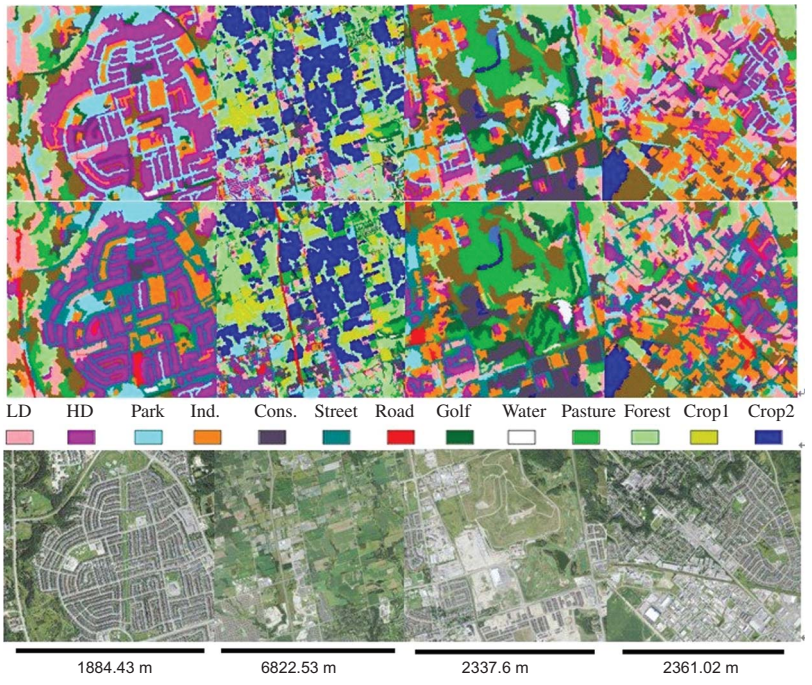

Figure 10. Selected samples of the classification results by compressed logarithmic Pauli parameters. Row 1, SVM results; Row 2, SVM combined rules; Row 3, corresponding ground truths.

This is the first study on the analysis of multi-temporal dual-orbital RADARSAT-2 polarimetric SAR data for urban land-cover mapping. The major contributions of our research can be summarized as follows.

- We have presented a detailed urban analysis with more urban land-cover classes, while most of the previous studies only focused on the extractions of the urban extent (Lombard et al. 2003; Zhang et al. 2010; Gamba, Aldrighi, and Stasolla 2011) or on mapping very few urban classes (Pellizzeri 2003; Alberga, Satalino, and Staykova 2008; Zhu et al. 2011). Only one previous study performed a detailed urban land-cover mapping using object-based SVM on multi-temporal single polarization RADARSAT-1 SAR data (Hu et al. 2008a). Our research showed that detailed urban classes could be mapped using high-resolution polarimetric SAR data with high accuracy through object-based SVM. Further, the efficiency of SVM with a limited number of training samples was evaluated by Foody and Mathur (2004) using a pixel-based approach. We have demonstrated that the object-based SVM is also effective with limited training samples.
- More polarimetric SAR features and their pre-processed forms have been studied for detailed urban land-cover mapping using an object-based rule-based approach. Although two previous studies compared more polarimetric parameters (Alberga 2007, Alberga, Satalino, and Staykova 2008), they had only two urban classes and used single-date airborne SAR data with pixel-based classification.

Table 8. Comparison of our results with those of previous urban mapping studies using polarimetric SAR data.

Sensor/frequency/pixel spacing (or spatial resolution)	Polsar features studied	Temporal/orbits	Urban/non-urban classes*	Best OA, kappa (%)	Classification method	Reference
RADARSAT-2/C-band/5.1 × 4.7 m	Freeman, Pottier, Pauli decomposition parameters; coherency matrix; HH, HV, VV intensities; corresponding pre-processing forms	6 dates/asc and des (40°–41°)	6/7	0.90, 0.89	Object-based Rule-based	Ours
SIR-C/C- and L-band/12.5 × 12.5 m	(No decomposition parameters.) Covariance matrix	1 date/no	1/2	0.83	Object-based	Lombard et al. (2003)
SIR-C/C-, L- and X-band/12.5 × 12.5 m	(No decomposition parameters.) HH, HV, VV intensities	3 dates/44°–57°	1/2	0.9	Pixel- and object-based	Pellizzeri et al. (2003)
AIRSAR/C- and L-band/6.7 × 12.1 m	Pottier decomposition parameters.	1 date/no	2/3	0.68	Object-based	Pellizzeri (2003)
E-SAR/L-band/0.89 × 1.5 m	8 polarimetric parameter sets	1 date/no	2/5	0.87, 0.85	Pixel-based	Alberga (2007)

(*Continued*)

Table 8. (Continued).

Sensor/frequency/pixel spacing (or spatial resolution)	Polsar features studied	Temporal/orbits	Urban/non-urban classes*	Best OA, kappa (%)	Classification method	Reference
E-SAR/L-band/0.89 × 1.5 m	19 polarimetric parameter sets	1 date/no	2/5	0.74, 0.69	Pixel-based	Alberga, Satalino, and Staykova (2008)
EMISAR/C- and L-band/2 × 2 m (spatial resolution)	MCSM*, Cameron decomposition parameters; HH, HV, VV intensity textures	6 dates/no studies on the combination form	1/4	0.85	Pixel-based	Zhang et al. (2010)
E-SAR/L-band/2.2 × 3 m (spatial resolution)	Various polarimetric interferometric parameters	Two data one date/no	1/6	0.93 (building accuracy)	Pixel-based	Li et al. (2010)
PALSAR/L-band/3.2 × 9.4 m	(No decomposition parameters.) HH, HV intensities and their textures	9 dates/all in 39°	3/14	0.72	Pixel-based	Zhu et al. (2011)
ERS-1/2/C-band/12.5 × 12.5 m (and simulated X-band data)	(No decomposition parameters.) Intensities	7 dates/(simulated data in three angles)	1/2	0.89	Pixel- based	Dell'Acqua, Gamba, and Lisini (2003)

Notes: *MCSM is multiple-component scattering model which is proposed in Zhang et al. (2010). Urban classes here represent man-made structures only. Water bodies, parks, golf course and other vegetation classes are grouped into non-urban classes. In our article, the six urban classes include high-density and low-density built-up areas, industrial/commercial area, construction sites, major roads and streets. Zhu et al. (2011) considered urban classes to include high-density and low-density areas and industrial/commercial areas. In Alberga (2007) and Alberga, Satalino, and Staykova (2008), urban classes include houses and roads. Li et al. (2010) have counted only building. Pellizzeri et al. (2003) have considered urban and sub-urban classes. The rest of the articles have only one class called 'urban' or 'building'.

Two previous studies used an object-based approach: one study investigated only SAR intensities (Pellizzeri et al. 2003) and the other used Pottier decomposition parameters for mapping fewer urban classes (Pellizzeri 2003).

- We have investigated the efficiencies of the temporal/orbital combinations of the polarimetric SAR data for urban land-cover classification, taking into account the temporal relationship and the orbital complement. Most of the previous urban studies assumed that multi-temporal data could generate better results, but no comparisons were conducted among multi-date combinations (Hu et al. 2008a, 2008b, Zhang et al. 2010; Zhu et al. 2011). A few comparative studies (Pellizzeri et al. 2003, Ban and Wu 2005) demonstrated that the results could be improved by additional data, but the efficiency of the combinations taking into account the temporal relationships was not investigated. Only one study showed that more streets can be detected and extracted using simulated multi-angle data (Dell'Acqua, Gamba, and Lisini 2003), but no studies were found on multi-angle/orbit SAR data for detailed urban land-cover mapping. Therefore, our study not only confirms the findings of previous studies that improvement could be achieved by additional data, but it also discusses the suitability of additional data.

5. Conclusion

This research investigated multi-temporal high-resolution RADARSAT-2 polarimetric SAR data for detailed urban land-cover mapping using an object-based SVM and a rule-based approach. Addressing the specific objectives stated in Section 1, the following conclusions can be drawn.

(1) For the object-based approaches, proper pre-processing of the data is essential for successful segmentation and classification. Appropriate filtering, logarithm and compression could improve the segmentation and classification results. Pauli parameters were found to be effective among the other polarimetric parameters. The compressed logarithmic filtered Pauli parameters have the best performance. The Cloude–Pottier parameters yielded lower accurate mapping, while the Freeman parameters and coherency matrix could generate similar good outcomes as the logarithmic intensity data.

(2) The object-based SVM could generate good classification results with limited training samples. The SVM and rule-based multi-temporal classification can map detailed urban land-cover classes with a high accuracy. An overall accuracy of 0.90 and kappa coefficient of 0.89 could be achieved by using the compressed logarithmic filtered Pauli parameters for segmentation and using such parameters from all the dates for classification.

(3) Better results could be achieved by adding more multi-temporal data. Although the best result (kappa = 0.91) is achieved on the six-date data set, very good results (kappa = 0.86) could be achieved using three-date combinations with data from both ascending and descending orbits with longer temporal span. The results indicate that complement information from ascending and descending orbits and the temporal relationship between the SAR data are significant when considering the efficiency of multi-temporal SAR data combination.

This research is one of the first studies on the analysis of multi-temporal dual-orbital space-borne polarimetric SAR data for detailed urban land-cover mapping using object-based SVM in combinations of rules.

Acknowledgements

The authors thank the Swedish National Space Board for funding this research and the Canadian Space Agency for providing the RADARSAT-2 polarimetric SAR data through the SOAR programme.

References

Agresti, A. 1996. *An Introduction to Categorical Data Analysis*, 312 p. New York: Wiley.

Ainsworth, T. L., D. L. Schuler, and J.-S. Lee. 2008. "Polarimetric SAR Characterization of Man-Made Structures in Urban Areas Using Normalized Circular-Pol Correlation Coefficients." *Remote Sensing of Environment* 112: 2876–85.

Alberga, V. 2007. "A Study of Land Cover Classification Using Polarimetric SAR Parameters." *International Journal of Remote Sensing* 28: 3851–70.

Alberga, V., G. Satalino, and D. K. Staykova. 2008. "Comparison of Polarimetric SAR Observables in Terms of Classification Performance." *International Journal of Remote Sensing* 29: 4129–50.

Baatz, M., and A. Schäpe. 2000. "Multiresolution Segmentation – An Optimization Approach for High Quality Multi-Scale Image Segmentation." In *Angewandte Geographische Informationsverarbeitung XII, Beiträge Zum AGIT-Symposium Salzburg*, 12–23,, Salzburg, June 30 edited by J. Strobl, T. Blaschke, and G. Griesebner. Heidelberg: Wichmann Verlag.

Ban, Y. 2003. "Synergy of Multitemporal ERS-1 SAR and Landsat TM Data for Classification of Agricultural Crops." *Canadian Journal of Remote Sensing* 29: 518–26.

Ban, Y., H. Hu, and I. M. Rangel. 2010. "Fusion of QuickBird MS and RADARSAT SAR Data for Urban Land-Cover Mapping: Object-Based and Knowledge-Based Approach." *International Journal of Remote Sensing* 31: 1391–410.

Ban, Y., and Q. Wu. 2005. "RADARSAT SAR Data for Landuse/Land-Cover Classification in the Rural–Urban Fringe of the Greater Toronto Area." In *Proceedings of the 8th AGILE Conference on Geographic Information Science,* Estoril, May 26–28, edited by F. Toppen, and M. Painho. Lisboa: Universidade Nova de Lisboa.

Blaschke, T. 2010. "Object Based Image Analysis for Remote Sensing." *ISPRS Journal of Photogrammetry and Remote Sensing* 65: 2–16.

Bradley, J. V. 1968. *Distribution-Free Statistical Tests*, 388 p. Englewood Cliffs, NJ: Prentice-Hall.

Buddhiraju, K. M., and I. A. Rizvi. 2010. "Comparison of CBF, ANN and SVM Classifiers for Object-Based Classification of High Resolution Satellite Images." In *IEEE International Geoscience and Remote Sensing Symposium*, 40–3, Honolulu, HI, July 25–30. Piscataway, NJ: IEEE.

Chang, C.-C., and C.-J. Lin. 2010. LIBSVM: A Library for Support Vector Machines (Accessed January 26, 2011). http://www.csie.ntu.edu.tw/~cjlin/libsvm/.

Cloude, S. R., and E. Pottier. 1997. "An Entropy Based Classification Scheme for Land Applications of Polarimetric SAR." *IEEE Transactions on Geoscience and Remote Sensing* 35: 549–57.

Cloude, S. R., and E. Pottier. 1996. "A Review of Target Decomposition Theorems in Radar Polarimetry." *IEEE Transactions on Geoscience and Remote Sensing* 34: 498–518.

Debeir, O., I. Van Den Steen, P. Latinne, P. Van Ham, and E. Wolff. 2002. "Textural and Contextual Land-Cover Classification Using Single and Multiple Classifier Systems." *Photogrammetric Engineering and Remote Sensing* 68: 597–605.

Definiens. 2011. Definiens Developer XD 1.5.2 Reference Book (Accessed July 5, 2011). http://workspace.imperial.ac.uk/imagingfacility/public/DefiniensReferenceBook.pdf.

Dell'acqua, F., P. Gamba, and G. Andlisini. 2003. "Improvements to Urban Area Characterization Using Multitemporal and Multiangle SAR Images." *IEEE Transactions on Geoscience and Remote Sensing* 41: 1996–2004.

Dixon, B., and N. Candade. 2008. "Multispectral Landuse Classification Using Neural Networks and Support Vector Machines: One or the Other, or Both?". *International Journal of Remote Sensing* 29: 1185–206.

Dong, Y., B. Forster, and C. Ticehurst. 1997. "Radar Backscatter Analysis for Urban Environments." *International Journal of Remote Sensing* 18: 1351–64.

Foody, G. F., and A. Mathur. 2004. "A Relative Evaluation of Multiclass Image Classification by Support Vector Machines." *IEEE Transactions on Geoscience and Remote Sensing* 42: 1335–43.

Freeman, A., and S. L. Durden. 1998. "A Three-Component Scattering Model for Polarimetric SAR Data." *IEEE Transactions on Geoscience and Remote Sensing* 36: 963–73.

Furberg, D., and Y. Ban. 2008. "Satellite Monitoring of Urban Sprawl and Assessing the Impact of Land Cover Changes in the Greater Toronto Area. In *21th ISPRS Congress*, *Technical Commission VIII,* 131–136, Beijing, July 3–11, edited by C. Jun, J. Jie and P. Ammatzia. Amsterdam: CRC Press.

Gamba, P., M. Aldrighi, and M. Stasolla. 2011. "Robust Extraction of Urban Area Extents in HR and VHR SAR Images." *IEEE Journal of Selected Topics in Applied Earth Observations and Remote Sensing* 4: 27–34.

Gao, Y., J.-F. Mas, B. H. P. Maathuis, X. M. Zhang, and P.M. Van Dijk. 2006. "Comparison of Pixel-Based and Object-Oriented Image Classification Approaches – A Case Study in A Coal Fire Area, Wuda, Inner Mongolia, China." *International Journal of Remote Sensing* 27: 4039–55.

Garcia, M., D. Riano, E. Chuvieco, J. Salas, and F. M. Danson. 2011. "Multispectral and LiDAR Data Fusion for Fuel Type Mapping Using Support Vector Machine and Decision Rules." *Remote Sensing of Environment* 115: 1369–79.

Guillaso, S., L. Ferro-Famil, A. Reigber, and E. Pottier. 2005. "Building Characterization Using L-Band Polarimetric Interferometric SAR Data." *IEEE Transactions on Geoscience and Remote Sensing* 2: 347–51.

Hsu, C. W., and C. J. Lin. 2002. "A Comparison of Methods for Multiclass Support Vector Machines." *IEEE Transactions on Neural Networks* 13: 415–25.

Hu, H., and Y. Ban. 2008a. "Urban Landuse/Land-Cover Mapping with High-Resolution SAR Imagery by Integrating Support Vector Machines into Object-Based Analysis." In *SPIE Conference on Remote Sensing for Environmental Monitoring, GIS Applications, and Geology VIII*, vol. 7110, 71100K1-8, Cardiff, September 15–18, edited by U. Michel, D. L. Civco, M.
Ehlers and H. J. Kaufmann. Bellingham, WA: SPIE.

Hu, H., and Y. Ban. 2008b. "Urban Land-Use Mapping and Change Detection with RADARSAT Fine-Beam SAR Data Using Neural Network and Rule-Based Classifiers." In *Proceedings of the XXI Congress of ISPRS*, *Technical Commission VII*, 1549–54, Beijing, July 3–11, edited by C. Jun, J. Jie, and J. van Genderen. Amsterdam: CRC Press.

Huang, C., L. S. Davis, and J. R. G. Townshend. 2002. "An Assessment of Support Vector Machines for Land Cover Classification." *International Journal of Remote Sensing* 23: 725–49.

Lardeux, C., P. L. Frison, C. Tison, J.-C. Souyris, B. Stoll, B. Fruneau, and J.-P. Rudant. 2009. "Support Vector Machine for Multifrequency SAR Polarimetric Data Classification." *IEEE Transactions on Geoscience and Remote Sensing* 47: 4143–52.

Lee, J. S. 1981. "Refined Filtering of Images Using Local Statistics." *Computer Graphics and Image Processing* 15: 380–9.

Lee, J. S., T. L. Ainsworth, J. P. Kelly, and C. Lopez-Martinez. 2008. "Evaluation and Bias Removal of Multilook Effect on Entropy/Alpha/Anisotropy in Polarimetric SAR Decomposition." *IEEE Transactions on Geoscience and Remote Sensing* 46: 3039–52.

Li, X., E. Pottier, H. Guo, and L. Ferro-Famil. 2010. "Urban Land Cover Classification with High-Resolution Polarimetric SAR Interferometric Data." *Canadian Journal of Remote Sensing* 36: 236–47.

Lombardo, P., M. Sciotti, T. M. Pellizzeri, and M. Meloni. 2003. "Optimum Model-Based Segmentation Techniques for Multifrequency Polarimetric SAR Images of Urban Areas." *IEEE Transactions on Geoscience and Remote Sensing* 41: 1959–75.

Lukin, V., N. Ponomarenko, A. Kurekin, K. Lever, O. Pogrebnyak, and L. P. Sanchez Fernandez. 2006. "Approaches to Classification of Multichannel Images." *Lecture Notes in Computer Science* 4225: 794–803.

Mcnairn, H., J. L. Shang, X. F. Jiao, and C. Champagne. 2009. "ALOS PALSAR Multipolarization and Polarimetric Data to Crop Classification." *IEEE Transactions on Geoscience and Remote Sensing* 47: 3981–92.

Moriyama, T., S. Uratsuka, T. Umehara, M. Satake, A. Nadai, H. Maeno, K. Nakamura, and Y. Yamaguchi. 2004. "A Study on Extraction of Urban Areas from Polarimetric Synthetic Aperture Radar Image." In *IEEE International Conference on Geoscience and Remote Sensing Symposium (IGARSS)*, 703–6, Anchorage, AK, September 20–24. Piscataway, NJ: IEEE.

Muller, K.-R., S. Mika, G. Ratsch, K. Tsuda, and B. Scholkopf. 2001. "An Introduction to Kernel-Based Learning Algorithms." *IEEE Transactions on Neural Networks* 12: 181–201.

Niu, X., and Y. Ban. 2010. "Multitemporal RADARSAT-2 Polarimetric SAR Data for Urban Land Cover Classification Using Support Vector Machine." In *30th EARSeL Symposium*, 581–8, Paris, 31 May–3 June 2010, edited by R. Reuter. Hannover: EARSeL.

Pal, M., and P. M. Mather. 2005. "Support Vector Machines for Classification in Remote Sensing." *International Journal of Remote Sensing* 26: 1007–11.

Pellizzeri, T. M. 2003. "Classification of Polarimetric SAR Images of Suburban Areas Using Joint Annealed Segmentation and '$H/A/\alpha$' Polarimetric Decomposition." *ISPRS Journal of Photogrammetry and Remote Sensing* 58: 55–70.

Pellizzeri, T. M., P. Gamba, P. Lombardo, and F. Dell'acqua. 2003. "Multitemporal/ Multiband SAR Classification of Urban Areas Using Spatial Analysis: Statistical Versus Neural Kernel-Based Approach." *IEEE Transactions on Geoscience and Remote Sensing* 41: 2338–53.

Rignot, E., R. Chellappa, and P. Dubois. 1992. "Unsupervised Segmentation of Polarimetric SAR Data Using the Covariance Matrix." *IEEE Transactions on Geoscience and Remote Sensing* 30: 697–705.

Trisasongko, B. H. 2010. "The Use of Polarimetric SAR Data for Forest Disturbance Monitoring." *Sensing and Imaging: An International Journal* 11: 1–13.

Tzotsos, A., and D. Argialas. 2008. "Support Vector Machine Classification for Object-Based Image Analysis." In *Object-Based Image Analysis – Spatial Concepts for Knowledge-Driven Remote Sensing Applications*, edited by T. Blaschke, S. Lang and G. J. Hay, 663–7. Berlin: Springer.

Waske, B., and J. A. Benediktsson. 2007. "Fusion of Support Vector Machines for Classification of Multisensor Data." *IEEE Transactions on Geoscience and Remote Sensing* 45: 3858–66.

Waske, B., and S. Van Der Linden. 2008. "Classifyingmultilevel Imagery from SAR and Optical Sensors by Decision Fusion." *IEEE Transactions on Geoscience and Remote Sensing* 46: 1457–66.

Zhang, L., B. Zou, J. Zhang, and Y. Zhang. 2010. "Classification of Polarimetric SAR Image Based on Support Vector Machine Using Multiple-Component Scattering Model and Texture Features." *EURASIP Journal on Advances in Signal Processing* 2010: 1–9.

Zhu, Z., C. Woodcock, J. Rogan, and J. Kellndorfer. 2011. "Assessment of Spectral, Polarimetric, Temporal, and Spatial Dimensions for Urban and Peri-Urban Land Cover Classification Using Landsat and SAR Data." *Remote Sensing of Environment* 117: 72–82.